# Detection of Alzheimer Pathology In Vivo Using Both $^{11}$C-PIB and $^{18}$F-FDDNP PET

Nelleke Tolboom[1,2], Maqsood Yaqub[1], Wiesje M. van der Flier[2], Ronald Boellaard[1], Gert Luurtsema[1], Albert D. Windhorst[1], Frederik Barkhof[3], Philip Scheltens[2], Adriaan A. Lammertsma[1], and Bart N.M. van Berckel[1]

*[1]Department of Nuclear Medicine and PET Research, VU University Medical Centre, Amsterdam, The Netherlands; [2]Department of Neurology and Alzheimer Centre, VU University Medical Centre, Amsterdam, The Netherlands; and [3]Department of Radiology, VU University Medical Centre, Amsterdam, The Netherlands*

$^{11}$C-Pittsburgh Compound-B ($^{11}$C-PIB) and $^{18}$F-(2-(1-{6-[(2-[$^{18}$F]fluoroethyl)(methyl)amino]-2-naphthyl}ethylidene) ($^{18}$F-FDDNP) have been developed as PET tracers for in vivo imaging of pathology in Alzheimer's disease (AD). The purpose of this study was to directly compare these tracers in patients with AD, patients with mild cognitive impairment (MCI), and healthy controls. **Methods:** Paired $^{11}$C-PIB and $^{18}$F-FDDNP scans were acquired in 14 patients with AD, 11 patients with amnestic MCI, and 13 controls. For both tracers, parametric images of binding potential ($BP_{ND}$) were generated. Global cortical $BP_{ND}$ was assessed using ANOVA. In addition, regional patterns of $BP_{ND}$ were compared between diagnostic groups using ANOVA for repeated measures. **Results:** Global cortical $BP_{ND}$ of $^{11}$C-PIB showed higher binding in patients with AD than in controls and patients with MCI. $^{18}$F-FDDNP uptake was higher in patients with AD than in controls, but MCI could not be distinguished from AD or from controls. Global $BP_{ND}$ values of both tracers were moderately correlated ($r = 0.45$; $P = 0.005$). In MCI, $BP_{ND}$ of $^{11}$C-PIB showed a bimodal distribution, whereas values for $^{18}$F-FDDNP were more widespread, with more MCI patients demonstrating increased uptake. Regional $^{11}$C-PIB binding showed different patterns across diagnostic groups, as AD patients showed an overall increase in binding, with the lowest binding in the medial temporal lobe. With $^{18}$F-FDDNP, patterns were similar across diagnostic groups. For all groups, highest values were observed in the medial temporal lobe. **Conclusion:** Differences in $BP_{ND}$ between patients with AD, patients with MCI, and controls were more pronounced for $^{11}$C-PIB. The difference in regional binding, the moderate correlation, and the discrepant findings in MCI suggest that they measure related, but different, characteristics of the disease.

**Key Words:** $^{11}$C-PIB; Pittsburgh Compound-B; $^{18}$F-FDDNP; positron emission tomography; PET; amyloid; Alzheimer disease

**J Nucl Med 2009; 50:191–197**
DOI: 10.2967/jnumed.108.056499

Received Jul. 30, 2008; revision accepted Oct. 30, 2008.
For correspondence or reprints contact: Nelleke Tolboom, Department of Neurology and Alzheimer Centre, VU University Medical Centre, P.O. Box 7057, 1007 MB, Amsterdam, The Netherlands.
E-mail: n.tolboom@vumc.nl


Alzheimer's disease (AD) is a progressive neurodegenerative disorder. The diagnosis of AD during life is based on clinical criteria, which have low sensitivity and specificity in the early stages of the disease (*1*). Mild cognitive impairment (MCI) is characterized by mild cognitive deficits; at the time of diagnosis, MCI patients do not have dementia, but they have an increased risk of progression to dementia (*2*). Ongoing developments in AD therapy dictate the need for developing techniques that identify subjects with incipient AD among patients with MCI. In vivo imaging of the pathology underlying AD holds promise for providing such a method.

Neuropathologically, AD is characterized by the accumulation of amyloid-β (Aβ) in senile plaques and hyperphosphorylated τ-protein in neurofibrillary tangles. Neurofibrillary tangles are thought to be present mainly in the medial temporal lobe (MTL) and lateral temporal lobe and, to a lesser extent, in the frontal, parietal, and occipital lobes. Amyloid plaques are more evenly distributed throughout the cortex, with relatively mild involvement of the hippocampal formation (*3*).

Over the past 2 decades, PET tracers have been developed for in vivo imaging of AD pathology. Of these ligands, $^{11}$C-Pittsburgh Compound-B (PIB) (*4*) and $^{18}$F-(2-(1-{6-[(2-[$^{18}$F]fluoroethyl)(methyl)amino]-2-naphthyl}ethylidene) malononitrile) ($^{18}$F-FDDNP) (*5*) have been used most widely.

First results with $^{11}$C-PIB showed greater cortical retention in patients with AD than in controls (*4,6–8*). This finding has been replicated several times in AD studies and has been extended to MCI patients in whom a more bimodal distribution has been described (*9–13*). It was also possible to distinguish between AD, MCI, and controls using $^{18}$F-FDDNP, but presently these findings have not been replicated (*5*).

Paired studies in the same subjects with validated tracer kinetic models are needed for a meaningful comparison. The aim of the present study was to directly compare global and regional uptake of $^{11}$C-PIB and $^{18}$F-FDDNP using validated quantitative methods in the same healthy controls and AD and MCI patients.

## MATERIALS AND METHODS

### Subjects

Fourteen AD patients, 11 amnestic MCI patients, and 13 healthy controls were included in this study. All subjects received a standard dementia screening that included medical history, physical and neurologic examinations, screening laboratory tests, brain MRI, and extensive neuropsychological testing. Among the neuropsychologic tests were the Mini Mental State Examination (MMSE) (*14*) and the Dutch version (*15*) of the Ray Auditory Verbal Learning Test (RAVLT) (*16*), a test specifically for episodic memory. Clinical diagnosis was established by the consensus of members of a multidisciplinary team, without knowledge of the PET results. All AD patients met criteria proposed by the National Institute of Neurological and Communicative Disorders and Stroke and the Alzheimer's Disease and Related Disorders Association (*17*) for "probable AD." Seven of the 14 AD patients were taking acetylcholine esterase inhibitors. Two AD patients used psychotropic medication (1 used a benzodiazepine and 1 a selective serotonin reuptake inhibitor). MCI patients met the Petersen criteria (*2*) based on subjective and objective cognitive impairment, predominantly affecting memory, in the absence of dementia or significant functional loss. Two patients with MCI used psychotropic medication (1 used a benzodiazepine and 1 a selective serotonin reuptake inhibitor). Controls were recruited through advertisements in newspapers and underwent the same diagnostic procedures; none of the controls used psychotropic medication.

Exclusion criteria were a history of major psychiatric or neurologic (other than AD) illness and the use of nonsteroidal anti-inflammatory drugs, because these have been reported to compete with $^{18}$F-FDDNP for binding to Aβ fibrils in vitro and to Aβ plaques ex vivo (*18*). Additional exclusion criteria for controls were subjective memory complaints or clinically significant abnormalities on the MRI (as determined by a neuroradiologist). Written informed consent was obtained from all subjects after a complete written and verbal description of the study. The study was approved by the Medical Ethics Review Committee of the VU University Medical Centre.

### PET

PET scans were obtained on an ECAT EXACT HR+ scanner (Siemens/CTI) equipped with a neuroinsert to reduce the contribution of scattered photons. This scanner enables the acquisition of 63 transaxial planes over a 15.5-cm axial field of view, thus allowing the whole brain to be imaged in 1 bed position. The properties of this scanner have been reported elsewhere (*19*). All subjects received a venous cannula for tracer injection. First, a 10-min transmission scan was acquired in 2-dimensional acquisition mode using 3 retractable rotating line sources. This scan was used to correct the subsequent emission scan for photon attenuation. Next, a dynamic emission scan in 3-dimensional acquisition mode was started simultaneously with the intravenous injection of $^{11}$C-PIB (351 ± 82 MBq), synthesized according to a modified procedure of Wilson et al. (*20*), with a specific activity of 41 ± 22 GBq/μmol using an infusion pump (Med-Rad; Beek) at a rate of 0.8 mL/s, followed by a flush of 42 mL of saline at 2.0 mL/s. This scan consisted of 23 frames increasing progressively in duration (1 × 15, 3 × 5, 3 × 10, 2 × 30, 3 × 60, 2 × 150, 2 × 300, 7 × 600 s), for a total frame duration of 90 min. Finally, after a resting period of at least 1 h to allow for decay of $^{11}$C, exactly the same procedure was repeated but now using an injection of $^{18}$F-FDDNP (177 ± 14 MBq) (*21*), with a specific activity of 86 ± 51 GBq/μmol. Patient motion was restricted by an immobilization device and monitored by laser beams that checked the position of the patient's head.

### MRI

All subjects underwent structural MRI using a 1.5-T Sonata scanner (Siemens). The scan protocol included a coronal T1-weighted 3-dimensional magnetization-prepared rapid-acquisition gradient echo (MPRAGE) (slice thickness, 1.5 mm; 160 slices; matrix size, 256 × 256; voxel size, 1 × 1 × 1.5 mm; echo time, 3.97 ms; repetition time, 2,700 ms; inversion time, 950 ms; flip angle, 8°), which was used for coregistration and region-of-interest (ROI) definition.

### Image and Data Analysis

All PET sinograms were corrected for dead time, tissue attenuation using the transmission scan, decay, scatter, and randoms and were reconstructed using a standard filtered backprojection algorithm and a Hanning filter with a cutoff at 0.5 times the Nyquist frequency. A zoom factor of 2 and a matrix size of 256 × 256 × 63 were used, resulting in a voxel size of 1.2 × 1.2 × 2.4 mm and a spatial resolution of approximately 7-mm full width at half-maximum at the center of the field of view. Images were then transferred to workstations (Sun Microsystems) for further analysis.

MR images were aligned to corresponding PET images using a mutual-information algorithm. Data were further analyzed using PVE-lab, a software program that uses a probability map based on 35 delineated ROIs that have been validated previously (*22*). No correction for partial-volume effects was applied to the PET data.

ROIs were projected onto $^{11}$C-PIB and $^{18}$F-FDDNP parametric images of binding potential ($BP_{ND}$). These parametric images were generated by applying a 2-step basis-function implementation of the simplified reference tissue model, with cerebellar gray matter as the reference tissue (RPM2) (*23*), to the full dynamic 90-min PET data. RPM2, a fully quantitative method for assessing the data, was identified as the parametric method of choice because it provided the best results for both tracers (*24,25*). The outcome measure $BP_{ND}$ is a quantitative measure of specific binding. It reflects the concentration of specifically bound tracer relative to the concentration of free and nonspecifically bound tracer in tissue under equilibrium (*26*). For regional analyses, $BP_{ND}$ of frontal (volume-weighted average of orbital frontal, medial inferior frontal, and superior frontal), parietal, and temporal (volume-weighted average of superior temporal and medial inferior temporal) cortices and MTL (volume-weighted average of enthorinal cortex and hippocampus) and posterior cingulate was used. In addition, a global cortical ROI was defined, based on the volume-weighted average of all these regions. Cerebellar gray matter was chosen as the reference tissue because of its (histopathologic) lack of Congo red– and thioflavin-S–positive plaques (*27,28*).

### Statistics

Data are presented as mean ± SD, unless otherwise stated. Differences between groups were assessed using ANOVA with post hoc LSD tests and age as a covariate. Associations between $^{11}$C-PIB and $^{18}$F-FDDNP were assessed using the Pearson correlation coefficient. The regional binding pattern of both $^{11}$C-PIB and $^{18}$F-FDDNP between subject groups was assessed using ANOVA for repeated measures with diagnosis as a between-subjects factor, brain region as a within-subjects factor, and age as a covariate. Separate models were run with $^{11}$C-PIB and $^{18}$F-FDDNP as

dependent variables. A $P$ value below 0.05 was considered significant.

## RESULTS

$^{11}$C-PIB and $^{18}$F-FDDNP studies were performed on the same day, except for 1 AD patient, 3 MCI patients, and 2 healthy controls, who were scanned with an average interval of 3 wk because of radiosynthesis failure. The 3 groups were similar with respect to age and sex (Table 1). MMSE scores were available for all subjects. AD patients had lower MMSE scores than did controls and MCI patients. MMSE scores between the latter 2 groups did not differ. The Dutch version of the RAVLT was performed in all subjects, except for 3 AD patients.

Visual inspection of the PET images (Fig. 1) confirmed the known high cortical $^{11}$C-PIB binding in AD, with predominantly white matter uptake in controls. The specific component of $^{18}$F-FDDNP was less distinct, and high binding was observed in the striatum and thalamus. The latter regions were not part of the average global cortical region.

Average global cortical $BP_{ND}$ for $^{11}$C-PIB was 0.85 ± 0.10 in patients with AD, 0.28 ± 0.29 in patients with MCI, and 0.11 ± 0.15 in controls (Fig. 2A). ANOVA, with an adjustment for age, showed a significant difference between groups ($P < 0.0001$). Post hoc LSD tests showed higher $^{11}$C-PIB binding in AD patients than in controls and MCI patients (both $P < 0.0001$). Furthermore, $^{11}$C-PIB binding in MCI patients differed from that in controls ($P = 0.03$). In AD, average $^{18}$F-FDDNP global cortical $BP_{ND}$ was approximately 9-fold lower than average $^{11}$C-PIB global cortical $BP_{ND}$. Values were 0.09 ± 0.02 in AD patients, 0.08 ± 0.05 in MCI patients, and 0.05 ± 0.03 in controls (Fig. 2B). ANOVA with adjustment for age showed a difference between groups ($P = 0.04$). Post hoc LSD testing showed higher global $^{18}$F-FDDNP $BP_{ND}$ in AD patients than in controls ($P = 0.01$), but $^{18}$F-FDDNP $BP_{ND}$ in MCI patients could not be distinguished from that in either AD patients ($P = 0.54$) or controls ($P = 0.07$). $^{11}$C-PIB $BP_{ND}$ in MCI patients appeared to be bimodal, with values similar to those in either AD patients or controls. In contrast, $^{18}$F-FDDNP $BP_{ND}$ values for MCI patients were quite dispersed; some MCI patients had lower values than most controls and others even had higher values than did AD patients. Across diagnostic groups, there was a moderate correlation of $BP_{ND}$ values between the 2 tracers ($r = 0.45$; $P = 0.005$; Fig. 3). Within diagnostic groups, however, there was no significant correlation (AD, $r = -0.18$; MCI, $r = 0.34$; controls, $r = 0.42$; all, $P > 0.15$). This discrepancy in binding between tracers within subjects is best demonstrated by 3 MCI patients, who, compared with the controls, displayed relatively high $^{18}$F-FDDNP uptake but similar $^{11}$C-PIB binding (Fig. 3).

There was a strong correlation between $^{11}$C-PIB and MMSE scores across diagnostic groups ($r = -0.75$; $P <$

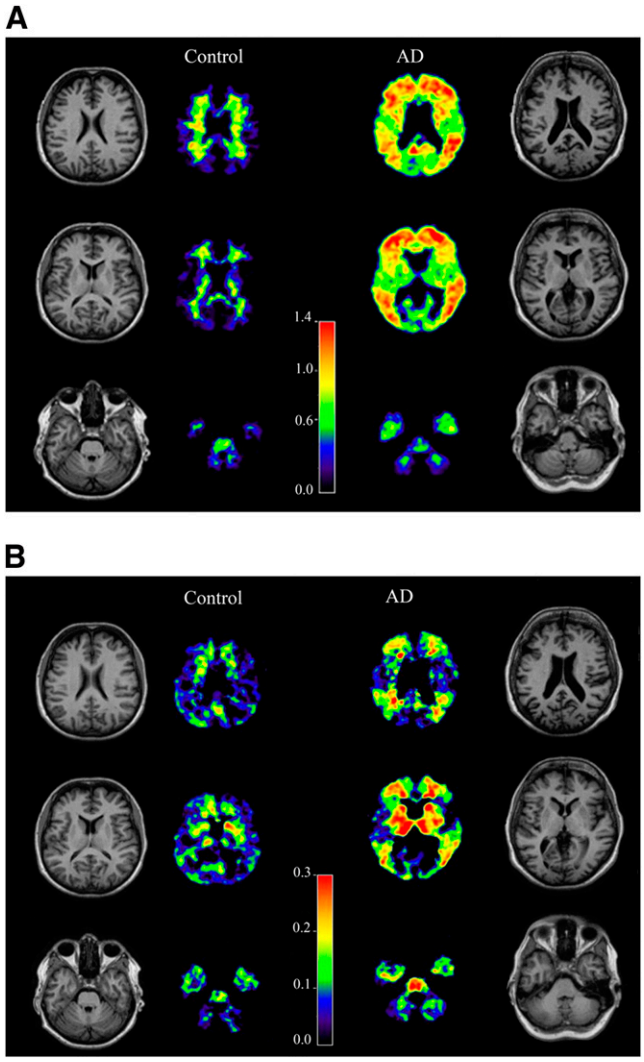


**FIGURE 1.** Examples of parametric $^{11}$C-PIB (A) and $^{18}$F-FDDNP (B) $BP_{ND}$ images in healthy control and AD patient. $^{11}$C-PIB and $^{18}$F-FDDNP scans were acquired in same subjects. In each panel, control is on the left and AD patient is on the right. High level of $^{18}$F-FDDNP binding in subcortical structures suggests nonspecific binding.

**TABLE 1.** Demographic and Clinical Characteristics According to Diagnostic Group

| Variable | Diagnostic group: Controls | MCI patients | AD patients | $P$ |
|---|---|---|---|---|
| Age (y) | 67 ± 7 | 68 ± 10 | 63 ± 7 | 0.21 |
| Percentage of women (F/M) | 39% (5/8) | 18% (2/9) | 43% (6/8) | 0.40 |
| MMSE | 29 ± 1 | 27 ± 3 | 23 ± 3 | <0.0001* |

*Post hoc LSD tests: AD < MCI, $P < 0.0001$; AD < Controls, $P < 0.0001$; MCI < Controls, $P = 0.15$.

Data are mean ± SD unless otherwise indicated. Differences between groups ($P$ value) were assessed using ANOVA.

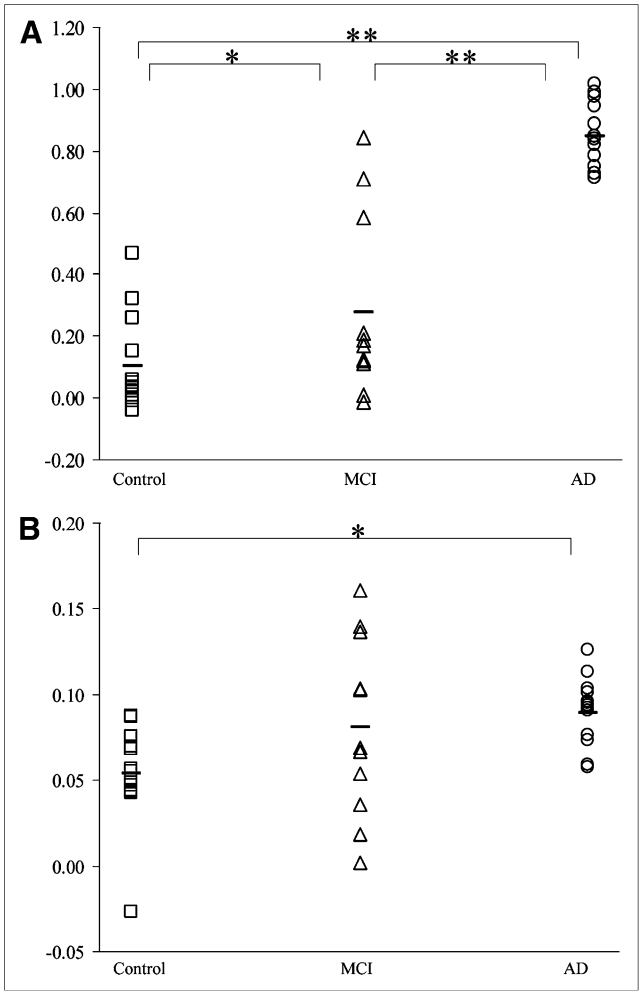


**FIGURE 2.** Scatter plots of global cortical $^{11}$C-PIB $BP_{ND}$ (A) and global cortical $^{18}$F-FDDNP $BP_{ND}$ (B), by diagnostic group. Horizontal lines between symbols represent mean values. Scale is 6-fold lower in B than in A. Differences between groups were assessed using ANOVA (adjusted for age, post hoc LSD correction). □ = controls; △ = MCI; ○ = AD. *$P < 0.05$. **$P < 0.0001$.

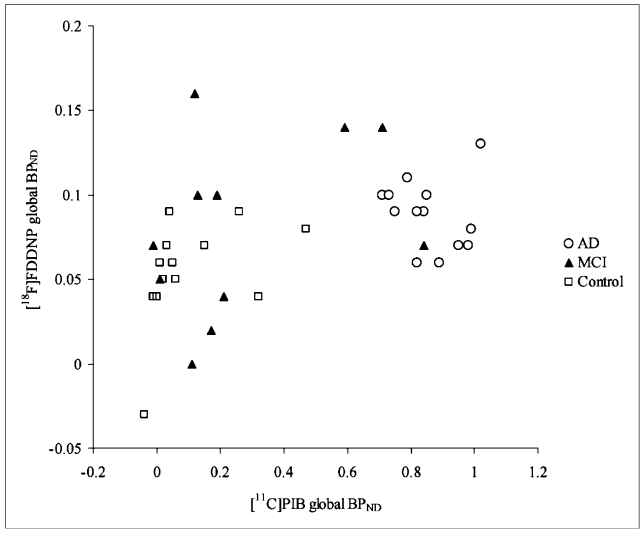


**FIGURE 3.** Correlation between $^{11}$C-PIB $BP_{ND}$ and $^{18}$F-FDDNP $BP_{ND}$. Across diagnostic groups, there was moderate correlation between $BP_{ND}$ values of the 2 tracers ($r = 0.45$; $P = 0.005$, Pearson correlation). Discrepancy in binding between tracers within subjects is best demonstrated by the 3 MCI patients at top of figure. Compared with controls, these 3 MCI patients displayed high $^{18}$F-FDDNP uptake but similar $^{11}$C-PIB binding.

0.0001). $^{18}$F-FDDNP showed a moderate correlation with MMSE ($r = -0.39$; $P = 0.02$) across groups. Furthermore, there was a strong correlation across diagnostic groups between $^{11}$C-PIB and the Dutch version of the RAVLT ($r = -0.63$; $P < 0.0001$). $^{18}$F-FDDNP showed a reasonably good correlation with the Dutch version of the RAVLT ($r = -0.47$; $P < 0.01$). Subsequently, regional binding patterns were investigated (Table 2; Fig. 4). In the case of $^{11}$C-PIB, ANOVA for repeated measures showed a significant main effect of diagnostic group ($P < 0.0001$) and brain region ($P = 0.02$). Moreover, an interaction between diagnostic group and brain region ($P < 0.0001$) was found, indicating different regional binding patterns between diagnostic groups. In controls, $^{11}$C-PIB binding was equal in all regions. Patients with AD, and to a lesser extent patients with MCI, showed markedly increased $^{11}$C-PIB binding in all regions, except in MTL, where binding was relatively low, compared with the uptake in the other regions (Fig. 4A). For $^{18}$F-FDDNP, there was a main effect of diagnostic group ($P = 0.05$) and region ($P = 0.001$). No interaction was found, indicating that regional differences were similar across diagnostic groups. AD patients, compared with controls, displayed an overall increase in binding, with MCI patients in between. Highest binding was seen in the (medial) temporal lobe and lower binding in the frontal, parietal, and posterior cingulate areas, with comparable patterns for the 3 diagnostic groups (Fig. 4B).

## DISCUSSION

This study directly compared global cortical and regional binding of $^{11}$C-PIB and $^{18}$F-FDDNP in the same AD and MCI patients and controls. Marked differences were revealed between the 2 tracers: global cortical binding of both tracers was only moderately correlated, binding in MCI patients varied between tracers, and regional binding patterns of both tracers differed substantially. These results all suggest that both tracers bind to different aspects of the neuropathology underlying cognitive decline associated with dementia.

Assessment of global cortical binding showed that both tracers were able to distinguish AD patients from controls on a group level. However, the specific binding of $^{11}$C-PIB in AD patients was substantially higher than that of $^{18}$F-FDDNP. Moreover, all AD patients displayed increased global cortical $^{11}$C-PIB binding without overlap with controls. In contrast, global cortical $^{18}$F-FDDNP binding in AD

**TABLE 2.** Regional $^{11}$C-PIB and $^{18}$F-FDDNP Binding ($BP_{ND}$) Data by Diagnostic Group

| | $^{11}$C-PIB | | | $^{18}$F-FDDNP | | |
|---|---|---|---|---|---|---|
| Brain region | Controls | MCI patients | AD patients | Controls | MCI patients | AD patients |
| Global | 0.11 ± 0.15 | 0.28 ± 0.29 | 0.85 ± 0.10 | 0.05 ± 0.03 | 0.08 ± 0.05 | 0.09 ± 0.02 |
| Frontal | 0.12 ± 0.21 | 0.31 ± 0.34 | 0.92 ± 0.10 | 0.05 ± 0.04 | 0.09 ± 0.07 | 0.10 ± 0.02 |
| Medial temporal | 0.07 ± 0.07 | 0.05 ± 0.08 | 0.15 ± 0.10 | 0.11 ± 0.03 | 0.13 ± 0.05 | 0.14 ± 0.05 |
| Temporal | 0.09 ± 0.12 | 0.26 ± 0.25 | 0.78 ± 0.11 | 0.07 ± 0.03 | 0.10 ± 0.06 | 0.10 ± 0.03 |
| Posterior cingulate | 0.11 ± 0.10 | 0.31 ± 0.29 | 0.80 ± 0.16 | 0.04 ± 0.04 | 0.06 ± 0.07 | 0.07 ± 0.05 |
| Parietal | 0.09 ± 0.13 | 0.29 ± 0.32 | 0.94 ± 0.18 | 0.03 ± 0.04 | 0.04 ± 0.04 | 0.06 ± 0.03 |

Data are mean ± SD.

patients showed substantial overlap with that in controls. This overlap is probably due to a higher level of nonspecific binding (binding other than to amyloid or tangles) in both groups, leading to a lower specific-to-nonspecific binding ratio. Consequently, at a group level differentiation is possible. However, identification of increased uptake in individual cases may prove to be difficult with $^{18}$F-FDDNP, but is possible with $^{11}$C-PIB. These results suggest that the accuracy of $^{18}$F-FDDNP as a differential diagnostic tool for detection of Alzheimer pathology in individual subjects will be lower than that of $^{11}$C-PIB.

For both tracers, MCI patients showed average binding intermediate between AD patients and controls. $^{11}$C-PIB binding in MCI patients was similar to that demonstrated in either controls or AD patients. This bimodal distribution of $^{11}$C-PIB binding in MCI patients is consistent with results from other studies (*10–13*). With $^{18}$F-FDDNP, the distribution of binding was more widespread. A larger number of MCI patients displayed increased global cortical $^{18}$F-FDDNP uptake, in some patients even exceeding that demonstrated in AD patients. In the only other report on $^{18}$F-FDDNP in MCI (*5*), MCI patients as a group showed intermediate $^{18}$F-FDDNP binding, and all patients displayed lower binding than that shown in AD patients with the highest binding, a finding that is somewhat discrepant with the present results and is probably due to patient selection.

Regional binding showed different patterns between the 2 tracers. For $^{11}$C-PIB, there was a difference in regional binding patterns between diagnostic groups. AD patients, compared with healthy controls, showed increased binding in all brain regions, with the smallest increase in the MTL. For $^{18}$F-FDDNP, regional binding patterns were comparable between diagnostic groups. AD patients, compared with controls, displayed an overall increase in binding, with MCI patients in between. For all 3 groups, highest values across brain regions were found in the MTL. The differences in regional binding can be explained by the binding characteristics of $^{11}$C-PIB and $^{18}$F-FDDNP: the in vivo cortical uptake of $^{11}$C-PIB primarily reflects Aβ-related cerebral amyloidosis (*29*), whereas uptake of $^{18}$F-FDDNP results from binding to both amyloid depositions and neurofibrillary tangles (*30*). The idea of different binding sites for $^{11}$C-PIB and $^{18}$F-FDDNP as a cause for differences in binding patterns is further supported by a recently published study comparing the 2 tracers in aged and young macaques (*31*). Relatively low binding of $^{11}$C-PIB in the MTL of AD patients is consistent with the low level of amyloid depositions in this region (*32*). Therefore, the relatively high binding of $^{18}$F-FDDNP in MTL suggests that this could be due to in vivo binding to neurofibrillary tangles, which are abundant in MTL. In the present study, 3 MCI patients displayed high $^{18}$F-FDDNP binding, and $^{11}$C-PIB binding was within the reference range. One can speculate that these MCI patients may have a prodromal dementia other than AD, for instance, a disease of the τ-proteins, contributing to the relatively high $^{18}$F-FDDNP uptake. Further studies are needed, however, to substantiate this hypothesis.

In general, the present results are in line with those reported in previous $^{11}$C-PIB studies (mostly expressed as distribution volume ratio, which equals $BP_{ND}$ + 1) (*4,8,11,33*). Previously published levels of global and regional binding (also expressed as distribution volume ratio) for $^{18}$F-FDDNP were slightly higher for AD (*5*); AD patients in the present study, however, were on average 10 y younger than those in the previously published study. Therefore, these differences could be due to differences in age, as tangle load has been reported to increase with age (*34*).

To date, 2 studies have compared both amyloid tracers in human subjects. The first study was performed in 2 different individuals with a hereditary prion disease, still making it difficult to provide an objective comparison of the 2 tracers (*35*). In a more recent study, Shin et al. (*36*) presented the first intrasubject comparison of $^{11}$C-PIB and $^{18}$F-FDDNP in healthy controls and AD subjects. They reported negligible $^{11}$C-PIB uptake but strong $^{18}$F-FDDNP uptake in the MTL in AD patients, whereas there was significant uptake of both tracers in neocortical areas. Although rather similar in design, there are several important differences in methods between this multitracer study and the present study. AD patients were, on average, 10 y older and had more severe AD with a mean MMSE score of 13. No MCI patients were included, and scans were performed on separate days. The average injected dose of $^{11}$C-PIB was similar, whereas the average injected dose of

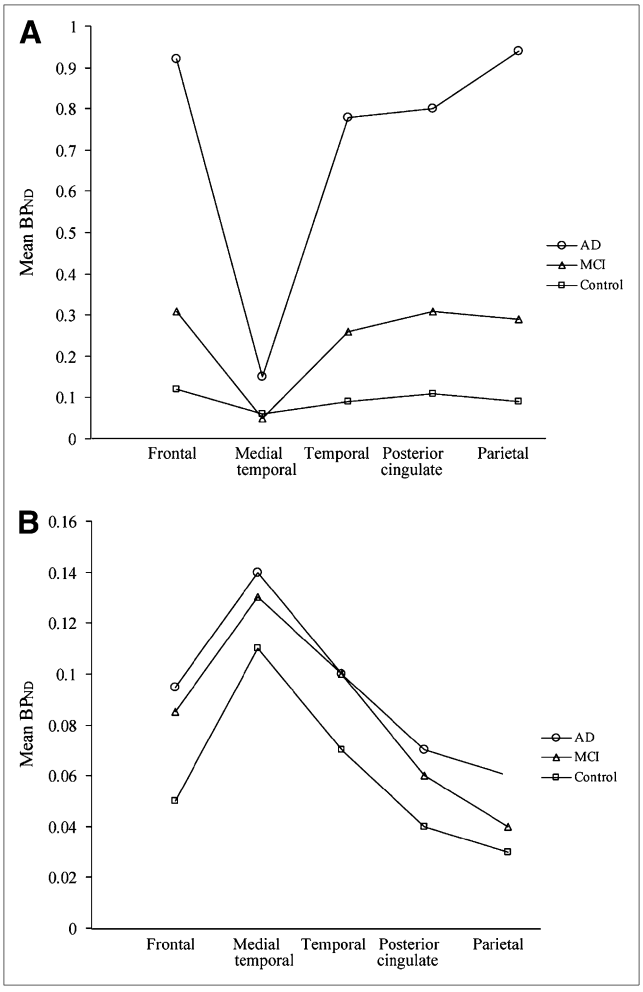


**FIGURE 4.** Regional binding pattern of both $^{11}$C-PIB (A) and $^{18}$F-FDDNP (B) between subject groups. Binding was assessed using ANOVA for repeated measures adjusted for age with diagnosis as between-subjects factor and brain region as within-subjects factor. Separate models were run with $^{11}$C-PIB and $^{18}$F-FDDNP as dependent variables. A *P* value below 0.05 was considered significant. Regional $^{11}$C-PIB binding pattern had significant main effect in subject group ($P < 0.0001$) and brain region ($P = 0.02$) and an interaction between subject group and brain region ($P < 0.0001$). Regional $^{18}$F-FDDNP binding pattern had significant main effect in subject group ($P = 0.05$) and brain region ($P = 0.001$), but without interaction.

$^{18}$F-FDDNP was lower. The total amount of injected $^{18}$F-FDDNP (labeled and nonlabeled) and thus the occupation of the number of binding sites, however, were approximately equal. PET data were analyzed using only semiquantitative methods. For $^{11}$C-PIB, standardized uptake value ratios ($SUV_r$), which is the target–to–gray matter cerebellar $SUV_r$ over the interval 40–60 min after injection, has been used to quantify PET data. Although this method has been validated for visualizing $^{11}$C-PIB accumulation (*7*), it may suffer from bias due to flow effects. Simple tissue ratios using 40- to 60-min data, such as $SUVR_{40–60}$, have been reported to overestimate specific binding by around 18% compared with a more quantitative model (*37*). $^{18}$F-FDDNP PET data have been quantified using $SUVR_{60–120}$. Currently, no formal validation of $SUVR_{60–120}$ has been published for $^{18}$F-FDDNP. The use of this nonvalidated analytic method for $^{18}$F-FDDNP warrants caution because a relatively small bias can lead to large effects in measured values due to the low specific-to-nonspecific binding ratio of $^{18}$F-FDDNP. Despite these essential differences, results were partly in line with each other. Levels of global and regional binding for $^{11}$C-PIB agreed well with the present study, for both controls and AD patients. However, levels of $^{18}$F-FDDNP binding were substantially higher globally and regionally in AD patients, and levels of $^{18}$F-FDDNP binding were substantially higher in the MTL in controls. Although most of the discrepancies found in the results could largely be attributed to differences in patient selection, as tangle load has been reported to increase with age (*34*) and disease severity (*38*), potential bias due to the use of nonvalidated analytic methods could also have confounded some of their results.

The main strength of the present study is its unique design, in which dynamic 90-min PET scans with both ligands were performed in the same patients along the spectrum of cognitive decline and on the same day. This design eliminated intersubject differences and thus enabled a balanced comparison.

Because of the longer radioactive decay of the $^{18}$F-labeled FDDNP (110 min), compared with $^{11}$C-PIB (20 min), the study was set up with $^{11}$C-PIB as the first scan. $^{11}$C-PIB with high specific activity was injected into tracer amounts (nanograms), leading to a negligible occupancy of $^{11}$C-PIB binding sites. In addition, analysis of the 6 patients for whom $^{11}$C-PIB and $^{18}$F-FDDNP scans were obtained on separate days, compared with $^{18}$F-FDDNP binding values of studies performed on a single day, revealed no difference of $^{18}$F-FDDNP binding. Therefore, it is highly unlikely that the order of the scans has influenced final results.

## CONCLUSION

The regional binding patterns, the moderately correlated global cortical binding, and the findings in MCI patients together imply that $^{11}$C-PIB and $^{18}$F-FDDNP measure related, but different, aspects of the neuropathology associated with AD. The binding of $^{18}$F-FDDNP to pathology other than amyloid may lead to its complementary use with $^{11}$C-PIB in the differential diagnosis of dementia. More specially, $^{18}$F-FDDNP might be useful in $^{11}$C-PIB–negative MCI patients, who could have prodromal dementias other than AD. Inclusion of more subjects, especially MCI patients, and clinical follow-up is needed to substantiate these findings.

## ACKNOWLEDGMENTS

We thank Anke A. Dijkstra for help with the data analysis, the PET radiochemistry and technology staff of the Division

of Nuclear Medicine and PET Research for tracer production and acquisition of PET data, and the technology staff of the Department of Radiology for acquisition of the MRI data. This work was financially supported by the Internationale Stichting Alzheimer Onderzoek (grant 05512), the American Health Assistance Foundation (grant A2005-026), and the FP6 network of excellence DiMI (LSH-2003-1.2.2.-2).

## REFERENCES


1. Cummings JL. Alzheimer's disease. *N Engl J Med.* 2004;351:56–67.
2. Petersen RC, Smith GE, Waring SC, Ivnik RJ, Tangalos EG, Kokmen E. Mild cognitive impairment: clinical characterization and outcome. *Arch Neurol.* 1999;56:303–308.
3. Braak H, Braak E. Neuropathological stageing of Alzheimer-related changes. *Acta Neuropathol.* 1991;82:239–259.
4. Klunk WE, Engler H, Nordberg A, et al. Imaging brain amyloid in Alzheimer's disease with Pittsburgh Compound-B. *Ann Neurol.* 2004;55:306–319.
5. Small GW, Kepe V, Ercoli LM, et al. PET of brain amyloid and tau in mild cognitive impairment. *N Engl J Med.* 2006;355:2652–2663.
6. Verhoeff NP, Wilson AA, Takeshita S, et al. In-vivo imaging of Alzheimer disease beta-amyloid with [$^{11}$C]SB-13 PET. *Am J Geriatr Psychiatry.* 2004;12:584–595.
7. Lopresti BJ, Klunk WE, Mathis CA, et al. Simplified quantification of Pittsburgh Compound B amyloid imaging PET studies: a comparative analysis. *J Nucl Med.* 2005;46:1959–1972.
8. Edison P, Archer HA, Hinz R, et al. Amyloid, hypometabolism, and cognition in Alzheimer disease: an [$^{11}$C]PIB and [$^{18}$F]FDG PET study. *Neurology.* 2007;68: 501–508.
9. Jack CR Jr, Lowe VJ, Senjem ML, et al. $^{11}$C PiB and structural MRI provide complementary information in imaging of Alzheimer's disease and amnestic mild cognitive impairment. *Brain.* 2008;131:665–680.
10. Kemppainen NM, Aalto S, Wilson IA, et al. PET amyloid ligand [$^{11}$C]PIB uptake is increased in mild cognitive impairment. *Neurology.* 2007;68:1603–1606.
11. Rowe CC, Ng S, Ackermann U, et al. Imaging beta-amyloid burden in aging and dementia. *Neurology.* 2007;68:1718–1725.
12. Forsberg A, Engler H, Almkvist O, et al. PET imaging of amyloid deposition in patients with mild cognitive impairment. *Neurobiol Aging.* 2008;29:1456–1465.
13. Price JC, Klunk WE, Lopresti BJ, et al. Kinetic modeling of amyloid binding in humans using PET imaging and Pittsburgh Compound-B. *J Cereb Blood Flow Metab.* 2005;25:1528–1547.
14. Folstein MF, Folstein SE, McHugh PR. "Mini-mental state": a practical method for grading the cognitive state of patients for the clinician. *J Psychiatr Res.* 1975;12:189–198.
15. Van der Elst W, Van Boxtel MPJ, Van Breukelen GJP, Jolles J. Rey's verbal learning test: normative data for 1,855 healthy participants aged 24-81 years and the influence of age, sex, education, and mode of presentation. *J Int Neuropsychol Soc.* 2005;11:290–302.
16. Rey A. *L'Examen Clinique en Psychologie.* Paris, France: PUF; 1964.
17. McKhann G, Drachman D, Folstein M, Katzman R, Price D, Stadlan EM. Clinical diagnosis of Alzheimer's disease: report of the NINCDS-ADRDA Work Group under the auspices of Department of Health and Human Services Task Force on Alzheimer's Disease. *Neurology.* 1984;34:939–944.
18. Agdeppa ED, Kepe V, Petri A, et al. In vitro detection of *S*-naproxen and ibuprofen binding to plaques in the Alzheimer's brain using the positron emission tomography molecular imaging probe 2-(1-[6-[(2-[$^{18}$F]fluoroethyl)(methyl)amino]-2-naphthyl]ethylidene)malono nitrile. *Neuroscience.* 2003;117:723–730.
19. Brix G, Zaers J, Adam LE, et al. Performance evaluation of a whole-body PET scanner using the NEMA protocol. *J Nucl Med.* 1997;38:1614–1623.
20. Wilson AA, Garcia A, Chestakova A, Kung HF, Houle S. A rapid one-step radiosynthesis of the β-amyloid imaging radiotracer *N*-methyl-[$^{11}$C]2-(4′-methylaminophenyl)-6-hydroxybenzothiazole ([$^{11}$C]-6-OH-BTA-1). *J Labelled Comp Radiopharm.* 2004;47:679–682.
21. Klok RP, Klein PJ, van Berckel BN, Tolboom N, Lammertsma AA, Windhorst AD. Synthesis of 2-(1,1-dicyanopropen-2-yl)-6-(2-[$^{18}$F]-fluoroethyl)-methylamino-naphthalene ($^{18}$F-FDDNP). *Appl Radiat Isot.* 2008;66:203–207.
22. Svarer C, Madsen K, Hasselbalch SG, et al. MR-based automatic delineation of volumes of interest in human brain PET images using probability maps. *Neuroimage.* 2005;24:969–979.
23. Wu Y, Carson RE. Noise reduction in the simplified reference tissue model for neuroreceptor functional imaging. *J Cereb Blood Flow Metab.* 2002;22:1440–1452.
24. Yaqub M, Tolboom N, Boellaard R, et al. Simplified parametric methods for [$^{11}$C]PIB studies. *Neuroimage.* 2008;42:76–86.
25. Yaqub M, Boellaard R, Van Berckel BNM, et al. Evaluation of tracer kinetic models for analysis of [18F]FDDNP studies. *Mol Imaging Biol.* In press.
26. Innis RB, Cunningham VJ, Delforge J, et al. Consensus nomenclature for in vivo imaging of reversibly binding radioligands. *J Cereb Blood Flow Metab.* 2007;27:1533–1539.
27. Yamaguchi H, Hirai S, Morimatsu M, Shoji M, Nakazato Y. Diffuse type of senile plaques in the cerebellum of Alzheimer-type dementia demonstrated by beta protein immunostain. *Acta Neuropathol.* 1989;77:314–319.
28. Joachim CL, Morris JH, Selkoe DJ. Diffuse senile plaques occur commonly in the cerebellum in Alzheimer's disease. *Am J Pathol.* 1989;135:309–319.
29. Lockhart A, Lamb JR, Osredkar T, et al. PIB is a non-specific imaging marker of amyloid-beta (Abeta) peptide-related cerebral amyloidosis. *Brain.* 2007;130: 2607–2615.
30. Agdeppa ED, Kepe V, Liu J, et al. Binding characteristics of radiofluorinated 6-dialkylamino-2-naphthylethylidene derivatives as positron emission tomography imaging probes for β-amyloid plaques in Alzheimer's disease. *J Neurosci.* 2001;21(RC189):1–5.
31. Noda A, Murakami Y, Nishiyama S, et al. Amyloid imaging in aged and young macaques with [$^{11}$C]PIB and [$^{18}$F]FDDNP. *Synapse.* 2008;62:472–475.
32. Arnold SE, Hyman BT, Flory J, Damasio AR, Van Hoesen GW. The topographical and neuroanatomical distribution of neurofibrillary tangles and neuritic plaques in the cerebral cortex of patients with Alzheimer's disease. *Cereb Cortex.* 1991;1:103–116.
33. Engler H, Forsberg A, Almkvist O, et al. Two-year follow-up of amyloid deposition in patients with Alzheimer's disease. *Brain.* 2006;129:2856–2866.
34. Price JL, Morris JC. Tangles and plaques in nondemented aging and "preclinical" Alzheimer's disease. *Ann Neurol.* 1999;45:358–368.
35. Boxer AL, Rabinovici GD, Kepe V, et al. Amyloid imaging in distinguishing atypical prion disease from Alzheimer disease. *Neurology.* 2007;69:283–290.
36. Shin J, Lee SY, Kim SH, Kim YB, Cho SJ. Multitracer PET imaging of amyloid plaques and neurofibrillary tangles in Alzheimer's disease. *Neuroimage.* 2008;43:236–244.
37. Koeppe RA, Frey KA. Equilibrium analysis of [$^{11}$C]PIB studies. *Neuroimage.* 2008;41(suppl 2):T30.
38. Arriagada PV, Growdon JH, Hedleywhyte ET, Hyman BT. Neurofibrillary tangles but not senile plaques parallel duration and severity of Alzheimer's disease. *Neurology.* 1992;42:631–639.